LBL-14353
Preprint c.2

Lawrence Berkeley Laboratory
UNIVERSITY OF CALIFORNIA

Materials & Molecular Research Division

Submitted to the Journal of Nuclear Materials

THE UO_2 - ZIRCALOY CHEMICAL INTERACTION

D.R. Olander

April 1982

RECEIVED
LAWRENCE
BERKELEY LABORATORY

JUL 21 1982

LIBRARY AND
DOCUMENTS SECTION

TWO-WEEK LOAN COPY

This is a Library Circulating Copy
which may be borrowed for two weeks.
For a personal retention copy, call
Tech. Info. Division, Ext. 6782.

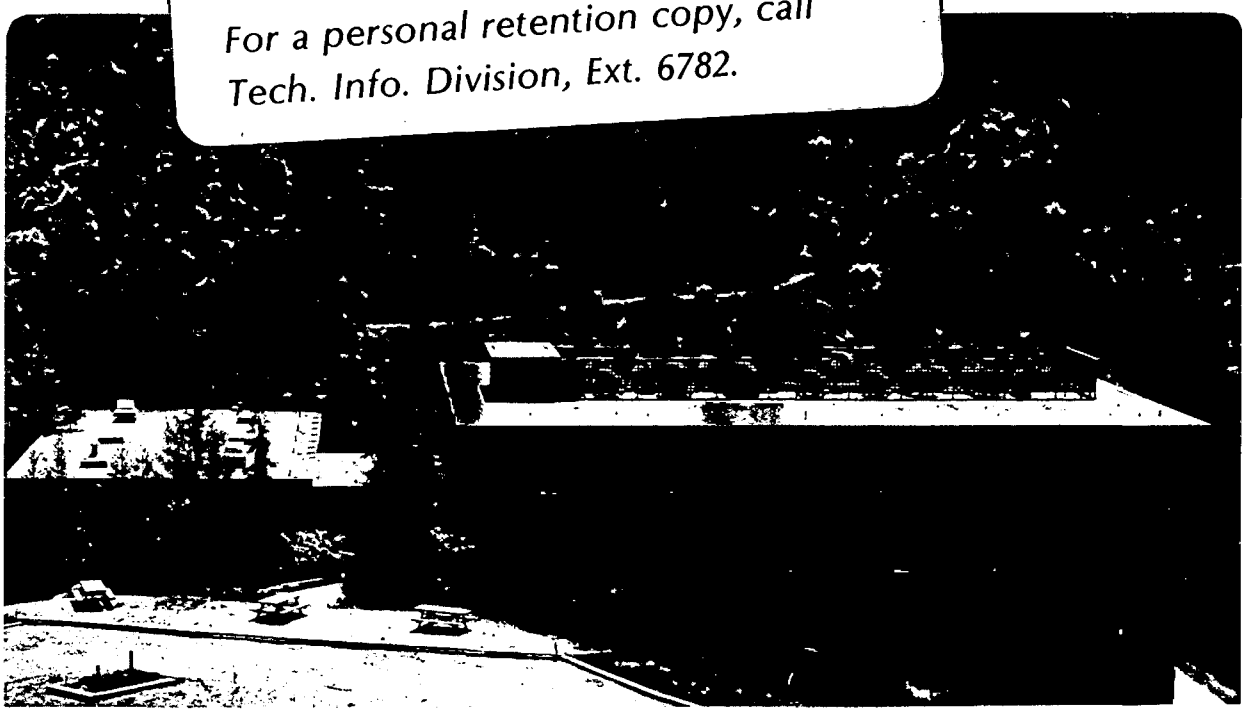

Prepared for the U.S. Department of Energy under Contract DE-AC03-76SF00098

LBL-14353 c.2

DISCLAIMER

This document was prepared as an account of work sponsored by the United States Government. While this document is believed to contain correct information, neither the United States Government nor any agency thereof, nor the Regents of the University of California, nor any of their employees, makes any warranty, express or implied, or assumes any legal responsibility for the accuracy, completeness, or usefulness of any information, apparatus, product, or process disclosed, or represents that its use would not infringe privately owned rights. Reference herein to any specific commercial product, process, or service by its trade name, trademark, manufacturer, or otherwise, does not necessarily constitute or imply its endorsement, recommendation, or favoring by the United States Government or any agency thereof, or the Regents of the University of California. The views and opinions of authors expressed herein do not necessarily state or reflect those of the United States Government or any agency thereof or the Regents of the University of California.

LBL-14353

THE UO_2 - ZIRCALOY CHEMICAL INTERACTION

by D. R. Olander

Materials and Molecular Research
Division of the Lawrence Berkeley
Laboratory and the
Department of Nuclear Engineering
University of California
Berkeley, California 94720

Submitted to the Journal of Nuclear Materials

This work was supported by the Director, Office of Energy Research, Office of Basic Energy Sciences, Materials Sciences Division of the U.S. Department of Energy under contract #DE-AC03-76SF00098.

ABSTRACT

Existing experimental data on the interaction of uranium dioxide and Zircaloy are analyzed with a model that accounts for the formation and growth of three corrosion layers between the oxide and the metal. The kinetics of the process are governed by diffusion of oxygen and uranium in the five-zone system with chemical equilibrium at four interfaces. Three of the zones consist of two elements and are treated by conventional scaling theory. Transport of all three elements (Zr, U, and O) occurs in the remaining two zones, one of which consists of two coexisting phases. Modeling of the system results in product layer growth rates which are in good agreement with the experimental results at 1500°C, which is the only temperature that both kinetic and thermodynamic information is available for application of the theoretical model.

INTRODUCTION

The chemical affinity of Zircaloy and UO_2 has been recognized since the early experimental work of Mallet(1) and Rooney and Grossman(2). Recent in-reactor tests at INEL(3) and laboratory experiments at KfK(4) have confirmed the earlier findings and provided more information on what is a very complex ternary corrosion process. As shown by these experiments, Zircaloy absorbs oxygen from UO_2 practically as readily as it does from steam, despite the vast difference in the oxygen potentials of these two oxidants. However, although steam is sufficiently oxidizing to produce a scale of ZrO_2 on the substrate metal, such a layer is not found on Zircaloy which has been contacted with UO_2. The oxygen potential of the two-phase UO_{2-x} + U system (5,6) is slightly more negative than that of the ZrO_{2-x} + Zr couple(7), so that the reaction $UO_2 + Zr = U + ZrO_2$ does not occur. However, as long as zirconium is not saturated with oxygen, it can reduce urania to its lower phase boundary; continued oxygen absorption by zirconium is accompanied by production of metallic uranium. Even though a zirconium oxide scale is not formed by contact with UO_2, the practical consequences of both the steam- and the UO_2-oxidation processes is the same, namely embrittlement of the metal by formation of the oxygen-rich α-Zr phase and by increase of the oxygen content of the β-Zr phase.

The laboratory tests reported by Hofmann and Politis(4) revealed the complexity of the UO_2-Zircaloy interaction. Microscopic examination of corrosion couples following tests lasting up to 1 hour at temperatures between 1000 and 1500°C showed a system of 5 zones and 4 interfaces. Of

the five phases, the two terminal zones are the original UO_2 and Zircaloy components of the couple and the intervening three zones are formed by the interaction. Figure 1, taken from Ref. 4, shows the characteristics of the layers from electron microprobe and optical microscope examination.

Zone 1 is a UO_2 phase, which Auger Electron Spectroscopy (AES) showed to contain only uranium and oxygen, but no zirconium. This result is not surprising, since the diffusivity of Zr^{+4} on the cation sublattice of UO_2 is probably of the same order of magnitude as uranium self diffusion in UO_2. The diffusion coefficient is probably less than 10^{-10} cm^2/s at the temperatures of the corrosion experiments, so that penetration of Zr into the UO_2 phase would therefore have been at most a few microns, which is small compared to the thicknesses of the corrosion layers. Zone 1 is thus effectively a binary uranium-oxygen phase with a fluorite structure. The light-shaded phase seen in the UO_2 part of the electron microprobe image in Fig. 1 is probably metallic uranium precipitated from the hypostoichiometric solid solution during cooldown following the experiment.

The AES results of Ref. 4 also indicate that no uranium is present in the zones labeled 2 and 3 in Fig. 1. Zone 2 is the oxygen-stabilized α-zirconium phase which is produced by oxygen absorption in the low-oxygen β-zirconium phase (zone 3). These two phases are identical to those observed following steam oxidation of Zircaloy(8).

The unique features of the UO_2-Zircaloy interaction are found in zones 4 and 5, which contain all three elements. Zone 5 is a uranium-rich metal alloy containing very little oxygen. It is probably molten during experiments at temperatures greater than ∿ 1200°C. Zone 4 consists of two phases, the preponderant one being a continuous phase composed of zirconium and oxygen which shows every evidence of being identical to the

material in Zone 2, namely α-Zr. Zone 4 also exhibits a discontinuous phase, which appears to connect Zones 1 and 5 by continuous stringers. This part of Zone 4 is rich in uranium, and is most likely the same alloy of which Zone 5 is composed. Zone 4 is a manifestation of the ternary nature of the interaction; two-phase layers are impossible in binary corrosion couples(9).

Cronenberg and El-Genk(10) presented a pseudo-binary analysis of the interaction which considers simple diffusion of oxygen in UO_2 and zirconium phases, the latter being divided up into α and β zones as in theoretical treatments of steam oxidation of Zircaloy(8). In this analysis, the two-phase zone 4 was effectively combined with zone 2, and zone 5 was ignored. Their treatment also assumed in existence of thermodynamically unjustifiable solid solutions in the UO_2 zone with O/U ratios well below the known lower phase boundary of this system. The need for a multicomponent, multizone analysis of the UO_2-Zircaloy interaction was pointed out by these authors.

The present analysis of the UO_2/Zr corrosion couple has several objectives. First it should be capable of rationalizing the layer sequence in terms of the ternary U-Zr-O phase diagram. Second, it should explain mechanistically how a layer of uranium-rich alloy becomes sandwiched between two α-Zr layers. Third, it must justify the formation of a two-phase zone. Finally, the model should be capable of predicting the growth kinetics of the three finite zones (numbers 2, 4 and 5 in Fig. 1) from knowledge of the thermodynamic and transport properties of the ternary U-Zr-O system. Unfortunately, reliable kinetic data are reported by Hofmann and Politis only up to 1400¼C, but the only ternary phase diagrams they give are isotherms at 1000, 1500, and 2000°C. The following analysis is

therefore restricted to 1500°C, using growth kinetics of the interaction layers extrapolated from lower temperatures to compare theory with experiment.

II THE DIFFUSION PATH

The diffusion path is the curve on an isothermal section of a ternary phase diagram joining the terminal phases of a diffusion couple and tracing the concentration and phase variations throughout the entire system. There is no requirement for the diffusion path to be a straight line between the terminal compositions; tortuous paths seem to be the rule rather than the exception. A diffusion path can be determined a postiori by comparing the structure of the interaction zone with the ternary phase diagram(9). However, a priori prediction of diffusion paths is still not possible(11). Hoffman and Politis(4) drew a straight line diffusion path on the U-Zr-O phase diagram connecting UO_2 and α-Zr, but this path does not match the phase arrangements observed in the diffusion couple.

Figure 2 shows the 1500°C section of the U-Zr-O phase diagram(4) on which has been drawn a diffusion path that reproduces the observed phase structure shown in Fig. 1. The terminal phases are assumed to be stoichiometric UO_2 and oxygen-free β-Zr. Zone 1 is a uranium-oxygen binary and so the diffusion path runs along the O-U side of the ternary phase diagram from $UO_{2.00}$ to the lower phase boundary at 1500°C, which is $UO_{1.97}$(12,13). From the corner of the single phase UO_2 region of the phase diagram, the diffusion path jumps across the central three-phase region. This jump represents the interface between zone 1 and zone 4 in Fig. 1 and terminates at point e on the border of the two-phase region α-Zr + L. The location of this point is dictated by the fraction of each phase in this region. The compositions of the equilibrium phases in Zone 4 are read from the ends

of the tielines (hypothetical ones shown dashed in Fig. 2) which are intersected by the diffusion path. From Fig. 1, the liquid (U,Zr) phase constitutes roughly one or two percent of the volume of zone 4, and this distribution does not appear to vary through the zone. To correctly represent the first observation, the diffusion path must enter the two-phase region quite close to point b' rather than point c, and to reflect the invariance of the relative proportions of the two phases, the diffusion path must cut the tie lines at approximately right angles. The oxygen concentration of the α-Zr phase in zone 4 changes from the value corresponding to point b' at the interface with zone 1 to the value at point b at the boundary with zone 5. The analogous composition of the coexisting (U,Zr) liquid changes from point c to point d.

Zone 5 is liquid at the annealing temperature. Because diffusion coefficients in liquid metals are probably at least an order of magnitude larger than in similar solid metals at the same temperature, concentration gradients in zone 5 are neglected. This means that zone 5 has no length on the diffusion path, and is represented by point d in Fig. 2. However, concentration gradients are assumed to be present in the liquid metal in zone 4. The reason for this difference in the treatment of transport in the liquid metal in the two zones is due to the relative areas of each. The area for solute diffusion via the liquid metal stringers in zone 4 is approximately two orders of magnitude smaller than it is in zone 5, so that concentration gradients could be much larger in the former than in the latter.

The diffusion path doubles back on itself from point d, passing through the two-phase zone and entering the single phase α-Zr region at

point b. Because of the observed absence of uranium in the α-Zr and β-Zr zones, the diffusion path moves immediately to the O-Zr side of the phase diagram. In zone 2 the diffusion path traverses the α-Zr region between point b and the point labeled α-β, which is in equilibrium with the point β-α in the β-Zr zone 3. This zone ends at the Zr corner of the phase diagram.

The diffusion path shown in Fig. 2 is consistent with the morphology of the UO_2 - Zircaloy diffusion couple shown in Fig. 1. It is not, however, consistent with the AES concentration profiles of zone 4 reported in Ref. 4 (Fig. 13). These show a continuous decrease in uranium and oxygen concentrations from the 1-4 interface to the 4-5 interface and a zirconium concentration variation in the opposite sense. This behavior is inconsistent with entry of the diffusion path into the α-Zr + L region, for neither the composition of the coexisting phases nor their relative proportions change sufficiently to account for the AES results. The AES concentration distributions suggest passage of the diffusion path through the α-Zr + UO_2 two-phase region of the phase diagram. If this were the case, the second (minor) phase in zone 4 seen in Fig. 1 would have to be UO_2, an assignment which appears to be visually unlikely. Moreover, zone 5 is unquestionably the (U,Zr) liquid labeled L in the phase diagram, and there is no way that a diffusion path crossing the UO_2 + α-Zr two-phase region could terminate in this liquid phase.

The inconsistency arising from the AES element profiles in zone 4 is therefore ignored in the following analysis, and modeling is based on the diffusion path shown in Fig. 2 and on the morphology seen in Fig. 1.

III INTERFACE AND BULK MOVEMENT

The 5-zone system which is observed when UO_2 is contacted with

Zircaloy at high temperatures is shown schematically in Fig. 3. Initially the system consists of a block of stoichiometric UO_2 of thickness L_{10} pressed against a block of β-Zr of thickness L_{30}. The thicknesses of these blocks are assumed to be infinite as far as the diffusion processes are concerned (i.e., the concentration perturbations never reach the outer extremeties of the system during the time of contact at the high temperature). Alternatively, the end faces of the blocks can be viewed as planes in the semi-infinite media which are fixed in the lattices of the two solids. Displacements of the end faces are equivalent to movements of the bulk solids.

The interface between liquid zone 5 and zone 2 is (arbitrarily) fixed in time. The five velocities indicated in Fig. 3 are measured with respect to this fixed plane and are considered to be positive in the directions drawn. The velocities of the bulk uranium in zone 1 and of the bulk zirconium in zones 2 and 3 are denoted by v_{UO_2} and v_{Zr}, respectively. The motion of the observable interfaces in the diffusion couple are designated by v_Δ for the boundary between zones 1 and 4, by v_ε for the growth of the liquid layer, and by v_δ for the progression of the α-β transformation interface. For modeling purposes, the duplex zone 4 is represented as parallel blocks of α-Zry and (U,Zr) liquid, the volume (or cross sectional area) fraction of the latter being denoted by f.

As a result of the interaction, the original UO_2 phase shrinks in thickness from L_{10} to L_1 and the β-Zr zone is reduced in size from L_{30} to L_3. The layers created by the reaction, numbers 2, 4 and 5, have thicknesses designated by δ, ξ and ε, respectively. The object of the analysis is to predict these quantities as functions of time.

The velocities and layer thicknesses are related by:

$$\frac{dL_1}{dt} = -(v_{UO_2} + v_\Delta) \qquad (1)$$

$$\frac{d}{dt} = v_\Delta - v_\varepsilon \qquad (2)$$

$$\frac{d\varepsilon}{dt} = v_\varepsilon \qquad (3)$$

$$\frac{d\delta}{dt} = v_\delta \qquad (4)$$

$$\frac{dL_3}{dt} = -(v_{Zr} + v_\delta) \qquad (5)$$

Conservation of uranium in the system yields:

$$C_U^{ox} L_{10} = C_U^{ox} L_1 + f\xi c_U + \varepsilon c_U$$

where C_U^{ox} is the concentration of uranium in UO_2 and c_U is the concentration of uranium in the (U,Zr) liquid alloy. Taking the time derivative of the above equation and using Eqs(1) - (5) yields:

$$v_{UO_2} = x_{\ell U} B(1-f) v_\varepsilon - (1 - x_{\ell U} Bf) v_\Delta \qquad (6)$$

where

$$x_{\ell U} = c_U / c_\ell \qquad (7)$$

is the atom fraction of uranium in the liquid metal and c_ℓ is the total atom density of this alloy (on an oxygen-free basis). The quantity B is given by:

$$B = c_\ell / C_U^{ox} \qquad (8)$$

The analogous zirconium balance in conjunction with Eqs(1) - (5) yields:

$$v_{Zr} = [1 - (1 - x_{\ell Z}E)f]v_{\Delta} - (1 - x_{\ell Z}E)(1-f)v_{\varepsilon} \qquad (9)$$

where

$$x_{\ell Z} = 1 - x_{\ell U} \qquad (10)$$

and

$$E = c_{\ell}/C_Z^o \qquad (11)$$

and C_Z^o is the concentration of zirconium atoms in zircaloy.

Equations (6) and (9) determine the bulk UO_2 and Zr velocities in terms of the interface velocities, reducing the number of unknowns to three.

Following the procedure applicable to binary diffusion problems in semi-infinite media(14), the interface velocities are assumed to behave parabolically:

$$v_{\delta} = k_{\delta}/\sqrt{t}$$

$$v_{\varepsilon} = k_{\varepsilon}/\sqrt{t} \qquad (12)$$

$$v_{\Delta} = k_{\Delta}/\sqrt{t}$$

The three quantities to be determined are the scaling coefficients k_{δ}, k_{ε}, and k_{Δ}.

IV OXYGEN DIFFUSION IN BINARY ZONES 1, 2 AND 3

The heavy curve in the bottom drawing of Fig. 3 represents the distribution of the concentration of oxygen in the various solid phases. Thermodynamic equilibrium is assumed at all interfaces, so that even though the concentrations exhibit discontinuities, the oxygen potential decreases continuously from left to right. The boundary concentrations indicated on the drawing are taken either from the ternary phase diagram of Fig. 2 or from the applicable binary phase diagram (i.e., the U-O system for C_a and the Zr-O system for $C_{\alpha\beta}$ and $C_{\beta\alpha}$). The oxygen concentration gradients

vanish well before the ends of the terminal UO_2 and β-Zr blocks, in accord with the assumption that these zones are semi-infinite as far as the diffusion process in concerned.

In zones 1, 2 and 3 of Fig. 3, oxygen conservation equations of the form:

$$\frac{\partial C_i}{\partial t} = - \nabla J_i \qquad (13)$$

apply, where J_i is the flux of oxygen with respect to the coordinate system selected for zone i. The coordinate axes shown in Fig. 3 are z, x, and y, for zones 1, 2 and 3, respectively, and the origins of the coordinate systems are at the bases of the coordinate arrows on the drawing. The fluxes J_i are composed of diffusive and convective components. The former represents movement of oxygen by molecular diffusion relative to the metal atom lattice. This component of the flux is described by Fick's first law. To this component must be added the convective flux of oxygen arising from movement of the host metal atom lattice with respect to the coordinate system axis. Thus:

$$J_i = - D_i \nabla C_i + v_{\ell i} C_i \qquad (14)$$

where D_i is the diffusion coefficient of oxygen in the medium of zone i, C_i is the oxygen concentration in this zone and $v_{\ell i}$ is the velocity of the metal atoms in zone i with respect to the reference coordinate system for this zone. Equation(14) is appropriate to binary systems, which, as explained earlier, characterizes zones 1, 2, and 3.

Zone 1

The origin of the coordinate system is chosen as the interface separating zones 1 and 4 and the coordinate is designated as z in Fig. 3. In this frame of reference, the velocity of the uranium atoms is:

$$v_{\ell 1} = -v_{UO_2} - v_{\Delta} = -k_1/\sqrt{t} \tag{15}$$

where, from Eqs(6) and (12),

$$k_1 = x_{\ell U} B[(1-f)k_{\varepsilon} + fk_{\Delta}] \tag{16}$$

The diffusion equation in zone 1 is:

$$\frac{\partial C_1}{\partial t} - \frac{k_1}{\sqrt{t}} \frac{\partial C_1}{\partial z} = D_1 \frac{\partial^2 C_1}{\partial z^2} \tag{17}$$

The boundary conditions are:

$$\begin{aligned} C_1(0,t) &= C_a \\ C_1(\infty,t) &= C_o \end{aligned} \tag{18}$$

and the initial condition is:

$$C_1(z,0) = C_o \tag{19}$$

The solution of Eq(17) subject to Eqs(18) and (19) is:

$$\frac{C_o - C_1}{C_o - C_a} = \frac{\operatorname{erfc}\left[\dfrac{z}{2\sqrt{D_1 t}} + \dfrac{k_1}{\sqrt{D_1}}\right]}{\operatorname{erfc}(k_1/\sqrt{D_1})} \tag{20}$$

Zone 2

In zone 2, the x-coordinate is measured from the fixed plane shown in Fig. 3 and the zirconium lattice velocity is:

$$v_{\ell 2} = -v_{Zr} = -k_2/\sqrt{t} \tag{21}$$

where, using Eqs(9) and (12),

$$k_2 = [1 - (1 - x_{\ell Z}E)f]k_\Delta - (1 - x_{\ell Z}E)(1-f)k_\varepsilon \qquad (22)$$

The oxygen diffusion equation in zone 2 is:

$$\frac{\partial C_2}{\partial t} - \frac{k_2}{\sqrt{t}}\frac{\partial C_2}{\partial x} = D_2 \frac{\partial^2 C_2}{\partial x^2} \qquad (23)$$

The boundary conditions are:

$$C_2(0,t) = C_b$$

and at $x = \delta = 2k_\delta\sqrt{t}$, (24)

$$C_2(2k_\delta\sqrt{t},t) = C_{\alpha\beta}$$

no initial condition is necessary because this zone does not exist at $t = 0$. The solution of Eqs(23) and (24) is:

$$\frac{C_2 - C_{\alpha\beta}}{C_b - C_{\alpha\beta}} = \frac{\operatorname{erfc}\left(\frac{x}{2\sqrt{D_2 t}} + \frac{k_2}{\sqrt{D_2}}\right) - \operatorname{erfc}\left(\frac{k_\delta + k_2}{\sqrt{D_2}}\right)}{\operatorname{erfc}\left(\frac{k_2}{\sqrt{D_2}}\right) - \operatorname{erfc}\left(\frac{k_\delta + k_2}{\sqrt{D_2}}\right)} \qquad (25)$$

<u>Zone 3</u>

In zone 3, the y coordinate moves with the α-β interface and the zirconium lattice velocity in this system is:

$$v_{\ell 3} = - v_\delta - v_{Zr} = -k_3/\sqrt{t} \qquad (26)$$

The oxygen diffusion equation for this zone is given by:

$$\frac{\partial C_3}{\partial t} - \frac{k_3}{\sqrt{t}}\frac{\partial C_3}{\partial y} = D_3 \frac{\partial^2 C_3}{\partial y^2}$$

The boundary conditions are:

$$C_3(0,t) = C_{\beta\alpha}$$
$$C_3(\infty,t) = 0 \qquad (27)$$

and the initial condition is:

$$C_3(y,0) = 0 \qquad (28)$$

The solution for the oxygen concentration distribution in zone 3 is:

$$\frac{C_3}{C_{\beta\alpha}} = \frac{\operatorname{erfc}\left(\frac{y}{2\sqrt{D_3 t}} + \frac{k_3}{\sqrt{D_3}}\right)}{\operatorname{erfc}(k_3/\sqrt{D_3})} \qquad (29)$$

V TRANSPORT IN ZONE 4

As shown in Fig. 3, zone 4 is modeling as a porous block of α-Zr penetrated by continuous stringers filled with a (U,Zr) liquid alloy containing a small concentration of oxygen. These channels and the all-liquid zone 5 provide high mobility transport pathways between the solid UO_2 of zone 1 and the solid α-Zr of zone 2. Both uranium and oxygen move from zone 1 down the liquid metal channels. In addition, oxygen migrates by solid state diffusion in the α-Zr phase of zone 4. Transport of oxygen and zirconium across the all-liquid zone 5 is assumed to take place with negligibly small concentration gradients.

Uraniuam transport in the (U,Zr) liquid stringers

Because oxygen is continously removed from the UO_2 phase while the O/U ratio at the 1-4 interface remains at the lower phase boundary of the oxygen-uranium system, there must be a flux of uranium across this interface.

Because of the low diffusion coefficient of uranium in solid zirconium and the low concentration of uranium in the α-Zr phase, the only pathways for uranium are the (U,Zr) liquid stringers in zone 4. Uranium is transported by diffusion and convection in these stringers and moves into zone 5 in this manner.

Since uranium does not diffuse in zone 1 (uranium self-diffusion in UO_2 is very slow at 1500°C), the flux of uranium across the 1-4 interface from zone 1 is purely convective and is equal to $(v_{UO_2} + v_\Delta)C_U^{ox}$. This flux is reckoned per unit of gross interfacial area. If all of the uranium in zone 4 moves along the (U,Zr) liquid channels, the flux in the stringers is increased by a factor of 1/f to account for the reduction in transport area which occurs as the uranium enters zone 4. The fractional area of transport in the stringers of zone 4 is equal to the volume fraction of the (U,Zr) phase in this two-phase zone. Thus the uranium flux in the liquid metal stringers of zone 4, measured in the coordinate system fixed to the 1-4 interface, is $(v_{UO_2} + v_\Delta)C_U^{ox}/f$. In this frame of reference, zirconium does not move because this element does not enter zone 1. Thus the uranium flux in the stringers is also equal to the total flux of liquid metal, and the flow velocity is obtained by dividing the flux by the density of the liquid metal (c_ℓ), which yields:

$$v_{\ell 4} = \frac{v_{UO_2} + v_\Delta}{fB} = \frac{k_{\ell 4}}{\sqrt{t}} \tag{30}$$

where B is given by Eq(8) and from Eq(15),

$$k_{\ell 4} = k_1/fB \tag{31}$$

The bulk velocity of the liquid metal in zone 4 varies as $t^{-\frac{1}{2}}$ because the

velocities v_{UO_2} and v_Δ exhibit this behavior.

The uranium flux in the (U,Zr) stringers in zone 4 is:

$$j_U = -D_\ell \frac{\partial c_U}{\partial \eta} + v_{\ell 4} c_U \tag{32}$$

where η is the coordinate measured from the 1-4 interface (Fig. 3). The mutual diffusion coefficient of the U-Zr liquid metal binary system is D_ℓ and c_U is the uranium concentration in the liquid metal. The diffusion/convection equation for uranium in the liquid phase of zone 4 is:

$$\frac{\partial c_U}{\partial t} + \frac{k_{\ell 4}}{\sqrt{t}} \frac{\partial c_U}{\partial \eta} = D_\ell \frac{\partial^2 c_U}{\partial \eta^2} \tag{33}$$

The boundary condition at $\eta = 0$ is the uranium concentration corresponding to point c in the ternary phase diagram (lower inset of Fig. 2):

$$c_U(0,t) = c_{Uc} \tag{34}$$

At the outer boundary of zone 4 at $\eta = \xi = 2(k_\Delta - k_\varepsilon)\sqrt{t}$, the uranium concentration is that corresponding to point d of the ternary phase diagram, the location of which remains to be determined. The boundary condition is:

$$c_U(\xi,t) = c_{Ud} \tag{35}$$

The solution of Eqs(33) - (35) is:

$$\frac{c_U - c_{Ud}}{c_{Uc} - c_{Ud}} = \frac{\operatorname{erf}\left(\dfrac{k_\Delta - k_\varepsilon - k_{\ell 4}}{\sqrt{D_\ell}}\right) - \operatorname{erf}\left(\dfrac{\eta}{2\sqrt{D_\ell t}} - \dfrac{k_{\ell 4}}{\sqrt{D_\ell}}\right)}{\operatorname{erf}\left(\dfrac{k_\Delta - k_\varepsilon - k_{\ell 4}}{\sqrt{D_\ell}}\right) + \operatorname{erf}\left(\dfrac{k_{\ell 4}}{\sqrt{D_\ell}}\right)} \tag{36}$$

The diffusive component of the flux at $\eta = 0$ is:

$$D_\ell\left(\frac{\partial c_U}{\partial \eta}\right)_{\eta=0} = -(c_{Uc} - c_{Ud})\frac{\sqrt{D_\ell}}{\sqrt{\pi t}}\frac{\exp(-k_{\ell 4}^2/D_\ell)}{\mathrm{erf}\left(\frac{k_\Delta - k_\varepsilon - k_{\ell 4}}{\sqrt{D_\ell}}\right) + \mathrm{erf}\left(\frac{k_{\ell 4}}{\sqrt{D_\ell}}\right)}$$

Because $k_{\ell 4} >> (k_\Delta - k_\varepsilon)$, this expression simplifies to:

$$D_\ell\left(\frac{\partial c_U}{\partial \eta}\right)_{\eta=0} = -\frac{(c_{Uc} - c_{Ud})D_\ell}{2(k_\Delta - k_\varepsilon)\sqrt{t}} \tag{37}$$

The uranium concentration in zone 5 (i.e., c_{Ud}) is determined by equating the uranium fluxes on the two sides of the 1-4 interface :

$$(v_{UO_2} + v_\Delta)C_U^{ox}/f = (j_U)_{\eta=0}$$

Using Eqs(30) - (32) and (37) yields:

$$k_1(C_U^{ox} - c_{Uc}/B) = \frac{fD_\ell(c_{Uc} - c_{Ud})}{2(k_\Delta - k_\varepsilon)} \tag{38}$$

Oxygen Transport in the (U,Zr) Liquid Stringers

In addition to uranium, oxygen is transported in the liquid metal stringers in zone 4 by a combination of molecular diffusion and convection. In the preceding analysis of uranium diffusion in this phase, the liquid metal was treated as a U-Zr binary liquid characterized by a concentration-independent mutual diffusion coefficient. This pseudo-binary approximation is acceptable because the concentration of oxygen in this phase is too low

to affect transport of the metal components. To describe oxygen diffusion in this liquid, on the other hand, the nonideality and the ternary properties of the system must be taken into account. The phenomenological description of ternary diffusion is discussed in detail by Kirkaldy and Brown(15) and by Roper and Whittle(16). The oxygen flux in the liquid metal can be written as:

$$j_O = -M \nabla\mu_O + v_{\ell 4} c_O \tag{39}$$

where the first term on the right hand side gives the molecular transport rate (with the solvent metal as a reference) and the second term represents convection of oxygen arising from motion of the metal with respect to the coordinate reference (the 1-4 interface). In Eq(39) M is the principal coefficient in the Onsager linear relation for the oxygen flux in a ternary mixture; the cross coefficients are neglected(16). The chemical potential of oxygen in the liquid metal is denoted by μ_O and is a function of the oxygen concentration c_O and the uranium concentration c_U. The zirconium concentration is not an independent variable. The oxygen chemical potential gradient in Eq(39) can be written as:

$$\nabla\mu_O = \left(\frac{\partial\mu_O}{\partial c_O}\right)\nabla c_O + \left(\frac{\partial\mu_O}{\partial c_U}\right)\nabla c_U \tag{40}$$

We make the assumption that the oxygen concentration in the liquid metal stringers of zone 4 is constrained to follow the phase boundary joining points c and a in the lower inset of Fig. 2. This restriction provides the following relation between the oxygen and uranium concentrations in the liquid metal:

$$\frac{c_O}{c_{Oc}} = \frac{c_U - c_{Ua}}{c_{Uc} - c_{Ua}} \tag{41}$$

where c_{Oc} is the oxygen concentration at point c and a is the termination of the phase boundary of the liquid zone on the U-Zr side of the phase diagram. This relationship permits ∇c_O in Eq (40) to be expressed in terms of ∇c_U, and the oxygen flux equation reduces to:

$$j_O = -D_{O\ell} \frac{\partial c_U}{\partial \eta} + v_{\ell 4} c_O \tag{42}$$

where $D_{O\ell}$ is the "practical" diffusion coefficient of oxygen in the liquid metal solvent:

$$D_{O\ell} = M \left(\frac{c_{Oc}}{c_{Uc} - c_{Ua}} \frac{\partial \mu_O}{\partial c_O} + \frac{\partial \mu_O}{\partial c_U} \right) \tag{43}$$

Oxygen transport in the α-Zr phase

In addition to transport by diffusion and convection in the liquid metal channels, oxygen migrates by solid state diffusion in the α-Zr phase of zone 4. Although the diffusion coefficient of oxygen in this phase is undoubtedly much smaller than it is in the parallel pathway provided by the liquid metal stringers, the area of the α-Zr phase is considerably larger than that afforded by the (U,Zr) liquid phase, so that the total oxygen flows in the two phases are of comparable magnitude.

Thermodynamic equilibrium is assumed to prevail at the extremities of zone 4. At the 1-4 interface, the oxygen content in the liquid metal stringers is that corresponding to point c in the ternary phase diagram (lower inset of Fig. 2). The oxygen content of the α-Zr phase at this interface is that given by point b' (upper right hand inset of Fig. 2). At the 4-5 interface, the oxygen content in the liquid metal channels is that corresponding to the uranium content c_{Ud} which is determined by Eq(38). Although the coexisting concentrations of the liquid and α-Zr

solid phases in the α-Zr + L two phase zone are not known, typical tie lines have been sketched on Fig. 2. Point d in the (U,Zr) liquid, which defines the composition of zone 5, is in equilibrium with point b in the α-Zr phase. Thus the oxygen concentration in the α-Zr phases which bound zone 5 are both equal to C_b. Oxygen diffusion in the α-Zr phase of zone 4 takes place in response to concentration difference $C_{b'} - C_b$.

The α-Zr part of zone 4 contains negligible uranium and can be treated as a Zr-O binary system which has the same properties as the material in zone 2. The thickness of this phase, ξ, increases with time due to zirconium which dissolves in the (U,Zr) liquid at the 2-5 interface and deposits at the 4-5 interface after transport across zone 5. Thus, the zirconium lattice in the α-Zr phase of zone 4 is not moving with respect to the 1-4 interface, so that oxygen diffusion is governed by the equation:

$$\frac{\partial C_4}{\partial t} = D_4 \frac{\partial^2 C_4}{\partial \eta^2} \tag{44}$$

where C_4 is the oxygen content of the α-Zr phase in zone 4 and $D_4 = D_2$ is the diffusion coefficient of oxygen in α-Zr. The boundary conditions for Eq(44) are:

$$\begin{aligned} C_4(0,t) &= C_b' \\ C_4(\xi,t) &= C_b \end{aligned} \tag{45}$$

where, using Eqs(2) and (12), $\xi = 2(k_\Delta - k_\varepsilon)\sqrt{t}$. The solution of Eqs(44) and (45) is:

$$\frac{C_4 - C_b}{C_b' - C_b} = \frac{\operatorname{erfc}\left(\frac{\eta}{2\sqrt{D_2 t}}\right) - \operatorname{erfc}\left(\frac{k_\Delta - k_\varepsilon}{\sqrt{D_2}}\right)}{1 - \operatorname{erfc}\left(\frac{k_\Delta - k_\varepsilon}{\sqrt{D_2}}\right)} \tag{46}$$

VI FLUX CONTINUITY CONDITIONS

The requirements that the component concentrations on adjacent sides of layer interfaces be those dictated by the appropriate phase diagram are contained in the solutions of the transport equations developed in Sections IV and V. In addition, three relations between the fluxes of oxygen and uranium at the system interfaces are needed to complete the theoretical description of the corrosion couple.

Oxygen Flux Match at the α-β Interface

The oxygen fluxes must be the same on both sides of the interface between zone 2 and zone 3. The oxygen flux in a coordinate system moving with the interface is the sum of the diffusive flux with respect to the metal lattice and the convective flux due to relative motion of the lattice atoms and the interface. With respect to the α-β interface in Fig. 3, the zirconium lattice moves from right to left with a velocity $v_\delta + v_{Zr}$. Noting that this sum is equal to $k_3/\sqrt{t}$(Eq(26)), the oxygen flux match is:

$$D_2\left(\frac{\partial C_2}{\partial x}\right)_{x=\delta} + \frac{k_3}{\sqrt{t}}\, C_{\alpha\beta} = D_3\left(\frac{\partial C_3}{\partial y}\right)_{y=0} + \frac{k_3}{\sqrt{t}}\, C_{\beta\alpha} \tag{47}$$

Oxygen Balance over Zones 4 and 5

The difference between the oxygen flux from zone 1 into zone 4 at the 1-4 interface and the oxygen flux into zone 2 at the 5-2 interface is equal to the time rate of change of the total amount of oxygen in zones 4 and 5. Based on the phase diagram of Fig. 2, the liquid (U,Zr) alloy

contains a negligible amount of oxygen compared to the quantity in the oxygen-saturated α-Zr phase. Thus the oxygen balance over zones 4 and 5 is:

$$-\left[-D_1\left(\frac{\partial C_1}{\partial z}\right)_{z=0} + v_{\ell 1}C_a\right] - \left[-D_2\left(\frac{\partial C_2}{\partial x}\right)_{x=0} + v_{\ell 2}C_b\right] = \frac{d}{dt}\left[(1-f)\xi\overline{C}_b\right]$$

Since the difference between the oxygen concentrations in the α-Zr phase at points b and b' in Fig. 2 is very small, the average concentration $\overline{C}_b$ on the right hand side can be replaced by C_b. The derivative $d\xi/dt$ which appears on the right hand side of the above balance is expressed in terms of the scaling coefficients by use of Eqs(2) and (12), which yields:

$$D_1\left(\frac{\partial C_1}{\partial z}\right)_{z=0} + \frac{k_1}{\sqrt{t}}C_a + D_2\left(\frac{\partial C_2}{\partial x}\right)_{x=0} + \frac{k_2}{\sqrt{t}}C_b = (1-f)C_b\frac{k_\Delta - k_\varepsilon}{\sqrt{t}} \qquad (48)$$

<u>Oxygen-to-Uranium flux ratio at the Interface between zones 1 and 4</u>

Because the O/U ratio of the UO_2 phase is very close to two even at the lower phase boundary, the ratio of the oxygen and uranium flows entering zone 4 from zone 1 must also be very nearly two. The oxygen flux into zone 4 consists of a component entering the α-Zr phase and another component carried in the liquid metal stringers. Uranium is transported only in the latter phase. The requirement that the ratio of these two element fluxes be equal to two leads to the relation:

$$(1-f)\left[-D_2\left(\frac{\partial C_4}{\partial \eta}\right)_{\eta=0}\right] + f(j_O)_{\eta=0} = 2f(j_U)_{\eta=0}$$

where the fluxes in each phase have been weighted by the fraction of the total area occupied by each. The fluxes of uranium and oxygen in the liquid

metal phase are given by Eqs(32) and (42), respectively. In these equations, the flow velocity $v_{\ell 4}$ is expressed in terms of the scaling constant k_1 by use of Eqs(30) and (31). The above equation becomes:

$$-\left(\frac{1-f}{f}\right)D_2\left(\frac{\partial C_4}{\partial \eta}\right)_{\eta=0} - (D_{O_\ell} - 2D_\ell)\left(\frac{\partial c_U}{\partial \eta}\right)_{\eta=0} = \frac{k_1}{fB\sqrt{t}}(2c_{Uc} - c_{Oc}) \tag{49}$$

VII NUMERICAL IMPLEMENTATION

The derivatives of Eq(47) are obtained from Eqs(25) and (29). Noting that according to Eqs(12), (21), and (26),

$$k_3 = k_\delta + k_2 \tag{50}$$

Eq(47) can be written as:

$$\frac{(C_b - C_{\alpha\beta})\exp(-S_{32}^2 A_3^2)}{\sqrt{\pi}\, S_{32}A_3\left[\mathrm{erfc}(A_2)-\mathrm{erfc}(S_{32}A_3)\right]} = \frac{C_{\beta\alpha}\exp(-A_3^2)}{\sqrt{\pi}\, A_3\,\mathrm{erfc}(A_3)} + (C_{\alpha\beta} - C_{\beta\alpha}) \tag{51}$$

where

$$S_{32} = (D_3/D_2)^{1/2} \tag{52}$$

$$A_2 = k_2/\sqrt{D_2} \tag{53}$$

$$A_3 = k_3/\sqrt{D_3} \tag{54}$$

With the concentration gradients determined by Eqs (20) and (25), Eq(41) becomes:

$$\frac{(C_o - C_a)\exp(-A_1^2)}{\sqrt{\pi}\, A_1\,\mathrm{erfc}(A_1)} + C_a + \frac{A_2C_b}{A_1S_{12}} = \frac{(C_b - C_{\alpha\beta})}{S_{12}A_1}\,\frac{\exp(-A_2^2)}{\mathrm{erfc}(A_2) - \mathrm{erfc}(S_{32}A_3)}$$

$$+ (1-f)C_b\left(\frac{k_\Delta - k_\varepsilon}{k_1}\right) \tag{55}$$

where

$$S_{12} = (D_1/D_2)^{1/2} \tag{56}$$

$$A_1 = k_1/\sqrt{D_1} \tag{57}$$

The difference in the scaling constants k_Δ and k_ε which appears in the last term of Eq(55) can be expressed in terms of k_1 and k_2 (or, equivalently, in terms of their dimensionless counterparts A_1 and A_2) by application of Eqs(16) and (22):

$$\frac{k_\Delta - k_\varepsilon}{k_1} = \frac{1}{1-f}\left(\frac{A_2}{S_{12}A_1} - \frac{1-(x_{\ell U})_c}{(x_{\ell U})_c}\,\frac{E}{B}\right) \tag{58}$$

The left hand side of this equation must be positive in order that the two-phase zone 4 exist in the corrosion couple. The uranium atom fraction in the liquid, $(x_{\ell U})_c$, is computed on an oxygen-free basis and is assumed to be that at point c in the phase diagram(Fig. 2).

The form of Eq(49) suitable for computation is obtained by using Eq(46) for the concentration gradient of oxygen in the α-Zr phase:

$$\left(\frac{\partial C_4}{\partial \eta}\right)_{\eta=0} = -\frac{(C_{b'} - C_b)}{\sqrt{\pi\, D_2 t}}\;\frac{1}{\operatorname{erf}\left(\dfrac{k_\Delta - k_\varepsilon}{\sqrt{D_2}}\right)} \tag{59}$$

The uranium concentration gradient in Eq(49) is given by Eq(37) in which the driving force $c_{Uc} - c_{Ud}$ is eliminated by use of Eq(38). Neglecting c_{Oc} compared to $2c_{Uc}$ on the right hand side of Eq(49), the O/U flux ratio condition becomes:

$$\frac{(1-f)(C_{b'} - C_b)}{\sqrt{\pi}\, C_o A_1 S_{12} \operatorname{erf}\left[\left(\dfrac{k_\Delta - k_\varepsilon}{k_1}\right) A_1 S_{12}\right]} + \left[1 - (x_{\ell U})_c\right]\left(\frac{1}{2}\,\frac{D_{O\ell}}{D_\ell} - 1\right) - (x_{\ell U})_c = 0 \tag{60}$$

where the condition for stoichiometric UO_2, $C_U^{ox} = C_o/2$, has been used.

Equations (51), (55), and (60) can be solved simulataneouly for the dimensionless scaling constants A_1, A_2, and A_3. Eq(58) is a subsidiary equation for this system, and Eq(38), written in the form:

$$\frac{2A_1^2}{fB}\left(\frac{k_\Delta - k_\varepsilon}{k_1}\right)\left(\frac{D_1}{D_\ell}\right) = \frac{(x_{\ell U})_c - (x_{\ell U})_d}{1 - (x_{\ell U})_c} \tag{61}$$

restricts the range of the solutions by requiring that point d in Fig. 2 lie along the phase boundary [i.e., the value of $(x_{\ell U})_d$ calculated from Eq(61) with given values of A_1 and A_2 must be larger than $(x_{\ell U})_a$].

Layer growth constants

The theory is best compared with experiment by calculating the kinetics of growth of the three finite zones (2, 4 and 5) in Figs. 1 and 3. The experimental results reported in Ref. 4 demonstrated parabolic growth of these three layers. This feature of the experimental behavior is already included in the model by virtue of the choice of the time dependences of the interface velocities (Eq(12)). However, the theory should also reproduce the magnitudes of the scaling rates. To facilitate this comparison the results of the model calculations are expressed in terms of growth constants, each of which is the thickness of a layer divided by the square root of time. For zones 2, 4, and 5, the growth constants are:

$$\begin{aligned} g_2 &= \delta/\sqrt{t} = 2k_\delta \\ g_4 &= \xi/\sqrt{t} = 2(k_\Delta - k_\varepsilon) \\ g_5 &= \varepsilon/\sqrt{t} = 2k_\varepsilon \end{aligned} \tag{62}$$

Using Eq(50), the growth constant of zone 2 is $2(k_3 - k_2)$, or in terms of the dimensionless parameters given by Eqs(52) - (54):

$$g_2 = 2\sqrt{D_2} \quad (S_{32}A_3 - A_2) \tag{63}$$

Using Eqs(56) - (58), the zone 4 growth constant is:

$$g_4 = \frac{2\sqrt{D_2}}{1-f} \left[A_2 - \frac{1 - (x_{\ell U})_c}{(x_{\ell U})_c} \frac{A_1 S_{12} E}{B} \right] \tag{64}$$

The theoretical growth constant for zone 5 requires solving Eqs(16) and (22) for k_ε in terms of k_1 and k_2. Using the dimensionless parameters of the model, the result is:

$$g_5 = \frac{2\sqrt{D_2}}{1-f} \left[\frac{1 - f\,[1 - \{1 - (x_{\ell U})_c\}E]}{(x_{\ell U})_c B} S_{12}A_1 - fA_2 \right] \tag{65}$$

VIII INPUT DATA NEEDED FOR THE MODEL CALCULATION

Theoretical prediction of the growth constants from the equations derived above requires specification of 15 thermodynamic, transport and structural parameters. Of these, 7 are from phase diagrams, 5 are diffusion coefficients, two involve material densities, and one is morphological.

Phase Diagram Data

The concentration of oxygen in stoichiometric UO_2 (which is not included in the 15 parameters discussed in the preceding paragraph) is assumed to be that of UO_2 with density of 10.9 g/cm^3, which is equivalent to C_o = 0.080 g atoms oxygen per cm^3.

The composition of urania at the lower phase boundary at 1500°C was determined from the results reported by Fryxell et al.(13) to be $UO_{1.97}$. This yields:

$$\frac{C_a}{C_o} = \frac{1.97}{2.0} = 0.985$$

In the ternary phase diagram of the Zr-U-O system at 1500°C shown in Fig. 2, the boundary between the α-Zr + L two-phase region and the single phase α-Zr region is shown as a point. In actuality, this boundary must have nonzero width, as indicated in the upper right hand inset in Fig. 2, which is our version of the phase diagram and not that of Hofmann and Politis(4). This liberty had to be taken because the entire model is unworkable if the segment b' - b in Fig. 2 is collapsed into a point; if $C_b = C_b'$, Eq(60) becomes a condition involving only input transport and thermodynamic properties of the system but is independent of the scaling parameters. In this case, Eq(60) is lost as the necessary third equation for determination of A_1, A_2 and A_3. The best estimate of the composition of the α-Zr corner of the central three-phase triangle in Fig. 2 is U/Zr/O = 0.028/0.710/0.262 (in atom fractions). The atom fraction of oxygen at this point (0.262) was converted to the volumetric concentration assuming that the density of oxygen-saturated α-Zr at 1500°C to be 6.41 g/cm^3 (17). This calculation yields $C_b' = 0.025$ g atoms oxygen/cm^3.

Although there is only a small uncertainty associated with this figure, the width of the boundary between the α-Zr + L and the α-Zr regions is totally unknown. However, the change in oxygen concentration between points b' and b on the phase diagram cannot be more than a few percent; a larger difference would probably have been experimentally detected. In principle, point b in Fig. 2 is connected via a tie line to point d, and once the latter has been determined (i.e., by Eq(61)), the former should follow from the phase diagram. However, the tie lines have not been determined, so the location of point b must be treated as a parameter which bears no operational relationship to point d. Therefore, C_b was considered to be an undetermined parameter, subject only to the restriction that it be

smaller than $C_{b'}$, but by no more than a few percent.

Zones 2 and 3 contain no uranium, so the equilibrium concentrations of oxygen in the two-phase α-Zr/β-Zr system can be taken from the Zr-O phase diagram. The values suggested by Pawel (8), $C_{\alpha\beta}$ = 0.0126 g atom oxygen/cm^3 and $C_{\beta\alpha}$ = 0.0058 g atoms oxygen/cm^3, were adopted.

The composition of point c in the U-Zr-O phase diagram was determined directly from Fig. 2. The oxygen content of the liquid phase is very small (<0.5 a/o) and the atom fraction of uranium is $(x_{\ell U})_c \simeq 0.71$. The uranium atom fraction at point a, $(x_{\ell U})_a$, is estimated to be 0.61 from Fig. 2. The accepted value from the binary phase diagram is 0.60 (18).

Material Densities

For the purpose of computing the density, the liquid metal phase was assumed to be 67 a/o U and 33 a/o Zr. These figures were used to calculate the weighted average of the densities of the pure component metals. The density of liquid uranium at 1500°C is 17.5 g/cm^3 (19). The density of liquid Zr at 1500°C was estimated from the density of the solid metal at its melting point(17), assuming a 2% volume increase on melting, and extrapolating the liquid metal density to 1500°C using the formula suggested by Strauss(20). The result is c_ℓ = 0.072 g atoms/cm^3. The density of uranium in UO_2 was taken to be one half of the oxygen density or C_U^{ox} = 0.040 g atom U/cm^3. Using these figures in Eq(8) gives B = 1.80. Taking the density of solid α-Zr from Ref. 17, the parameter E of Eq(11) is 1.02.

Diffusivities

A method of estimating the chemical diffusion coefficient of oxygen in UO_{2-x} is available(21). The resulting value of D_1 at 1500°C is 1.5×10^{-5} cm^2/s. The diffusion coefficients of oxygen in α-Zr and β-Zr suggested by Pawel(8) have been employed. At 1500°C, they are: D_2 = 2.0×10^{-6} cm^2/s and D_3 = 8.7×10^{-6} cm^2/s.

The mutual diffusion coefficient of the U-Zr liquid metal alloy was estimated as follows. The diffusivity of lanthanum in liquid uranium was measured at 1250°C to be 1.5×10^{-5} cm^2/s(22). This value was assumed to apply to the Zr-U system and extrapolated to 1500°C by assuming that the activation energy for liquid diffusion is equal to that of uranium viscosity, the latter being 6.5 kcal/mole(23). The best estimate of D_ℓ is thus 2.0×10^{-5} cm^2/s.

The practical diffusion coefficient of oxygen in the liquid metal (given by Eq(43)) is not known. It is probably larger than the diffusivity of the component metals in the liquid estimated in the preceding paragraph, but cannot be too large or Eq(60) has no solution.

Phase ratio in zone 4

The final parameter which needs to be specified for performing calculations with the theoretical model is the fraction of the (U,Zr) liquid phase in zone 4, (i.e., the parameter f). Based on the photomicrographs shown in Fig. 1, this phase occupies 1 - 2% of the total volume, which is an upper limit for the fraction of the cross sectional area available for transport along the liquid metal-filled channels in the model of zone 4.

IX COMPARISON WITH EXPERIMENT

Each of the input parameters required for the model calculations is associated with an uncertainty. Therefore, the theoretical calculations were made for ranges of each of the parameters centered on the best-estimate values given in the preceding section. In some instances, the uncertainty is given in the original source of the data, and is the case for diffusion in α-Zr (i.e., D_2). In most cases, the uncertainty range was based upon subjective assessment of the reliability of the original data and their applicability to the present problem. Thus information obtained from the

binary Zr-O phase diagram (i.e., $C_{\alpha\beta}$ and $C_{\beta\alpha}$) and from the U-O phase diagram (C_a) was judged to be more reliable than parameters taken from the phase diagram of Fig. 2. Diffusion coefficients which have been obtained by indirect means (i.e., D_1 and D_ℓ) are less certain than those which have been measured directly (D_2 and D_3). The density ratios B and E were judged to be quite accurate and so accorded small ranges of uncertainty. The estimate of the fraction of the two phases comprising zone 4 (the parameter f) was based solely on visual examination of the images in Fig. 1, and is probably not very reliable. For two parameters, C_b and $D_{O\ell}$, no information of any kind is available to make a priori estimates. However, the approximate values and ranges for these parameters are greatly restricted by the applicability of the entire method, as discussed in Section VIII.

Table 1 lists the input parameters, their most probable values, and the range accorded to each. Approximately 100 combinations were randomly selected for the 15 parameters within the allowable ranges and solution of Eqs(51), (55) and (60) attempted for each set. For three quarters of the parameter combinations, no solution was obtainable. The remaining sets of input parameters yielded solutions for the dimensionless scaling constants A_1, A_2 and A_3, from which the growth constants were computed from Eqs(63), (64) and (65). Of the 25 or so solutions, four resulted in growth constants which were in reasonable agreement with the experimental results. The parameters sets and resultant growth constants for these trials are shown in the last four columns of Table 1.

The experimental values of the growth constants at 1500°C are given in Fig. 16 of Ref. 4. In terms of the identification of the reaction layers used in Ref. 4. and the notation used here, zone 2 is the difference between layers III and II, zone 4 is layer I and zone 5 is the difference between

layers II and I. The values chosen for comparison with the model are those based on Arrhenius extrapolation of data at lower temperatures. The actual measured values at 1500°C (Table I of Ref. 4) are unavailable for zone 2 and 40 - 50% higher than the extrapolated values for zones 4 and 5. Comparison of the experimental values extrapolated from low temperatures with the range of the model predictions given in the last three rows of Table 1 is shown in Table 2. The deviations associated with the theoretical numbers arise from the averaging of the four calculational results in Table 1. These deviations reflect the uncertainties of the input parameters needed for the model computation, as listed in Table 1. The experimental growth constants for zones 2 and 4 fall within the range of the theoretical predictions. That for zone 5 is smaller than the theoretical value by $\sim$ 35%.

The thermodynamic and transport parameters which produce this agreement all cluster about the best estimates made in the preceding section. The difference between $C_{b'}$ and C_b in the final four cases reported in Table 1 ranges from 3% to 12%. Values of the other unknown parameter, the practical diffusion coefficient of oxygen in the liquid metal $D_{O\ell}$, is bracketed between 1.5 and 4.5 times the mutual diffusion coefficient of the binary metal system, D_ℓ. The theoretical results are very insensitive to the properties of the UO_2 phase. The deviation from perfect stoichiometry of UO_{2-x} appears only in the first term on the left hand side of Eq(55). This term is insignificant as long as C_a is close to C_o (e.g., if the O/U ratio of the oxide at the lower phase boundary of the uranium-oxygen system does not differ significantly from 2). For the same reason, the chemical diffusivity of oxygen in UO_{2-x} has virtually no influence on the layer growth rates. This property appears only in the first term on the left hand side of Eq(55)

(it is absent from the product A_1S_{12}, which occurs elsewhere in the equations of the model). Because this term is small compared to the others in this equation, sizeable variations in D_1 do not affect the growth constants even though the solution for the dimensionless parameter A_1 is changed.

The model is not capable of a priori prediction of the fraction f of the liquid metal phase in zone 4. Some unknown property of the system other than the ones used in the present model controls this feature. Figure 1 suggests that the liquid metal-filled channels in zone 4 are associated with grain boundaries of the coexisting α-Zr phase, so that interfacial energies may be involved in determining f. However, the values of the parameter obtained by treating it as an adjustable parameter in the four computational trials reported in Table 1 are certainly consistent with estimates of the volume fractions of the two phases from Fig. 1. Computations indicated that neither very small values of f (< 0.5%) nor very large values (> 5%) produced growth constants which matched the data, even when the other parameters were varied within their allotted ranges.

X CONCLUSIONS

Agreement between the observed and predicted layer growth constants is sufficiently good for all three zones to warrant acceptance of the theoretical model on which the computation is based. The material properties used in the theory all fall within ranges expected from estimates of these parameters.

ACKNOWLEDGEMENT

This work was supported by the Director, Office of Energy Research, Office of Basic Energy Sciences, Materials Sciences Division of the U.S. Department of Energy under contract #DE-AC03-76SF00098.

Table 1. Input Parameters and Results of Model Calculations*

Parameters	Best Estimate	Range	Computational Trial 1	2	3	4
C_a/C_o	.985	.980 - .988	.982	.981	.981	.984
$C_{b'}/C_o$	.313	.31 - .35	.345	.328	.335	.342
C_b/C_o	-	.30 - .33	.304	.302	.325	.313
$C_{\alpha\beta}/C_o$	.158	.140 - .170	.164	.155	.151	.165
$C_{\beta\alpha}/C_o$	.073	.060 - .080	.060	.076	.062	.075
$(x_{\ell U})_c$	.71	.65 - .75	.74	.75	.66	.68
$(x_{\ell U})_a$	.60	.58 - .64	.62	.60	.60	.60
$D_1 \times 10^5$	1.5	.4 - 4.0	1.2	1.3	.8	.8
$D_2 \times 10^5$	0.2	.15 - 0.25	.25	.24	.16	.16
$D_3 \times 10^5$	0.9	.4 - 2.0	1.2	1.5	1.8	1.6
$D_\ell \times 10^5$	2.0	1.0 - 4.0	1.7	3.4	2.1	3.5
$D_{O\ell} \times 10^5$	-	2.0 - 20.0	6.3	7.7	9.3	5.9
B	1.8	1.7 - 1.9	1.8	1.9	1.7	1.9
E	1.0	.9 - 1.1	1.0	1.0	0.9	1.0
f	.01 - .02	.005 - .04	.038	.020	.014	.033
g_2	-	-	13.2	16.0	18.7	17.5
g_4	-	-	6.8	3.7	4.0	4.0
g_5	-	-	3.9	3.2	3.0	2.2

* The units of diffusion coefficients are cm^2/s; the units of growth constants are $\mu m/s^{\frac{1}{2}}$.

Table 2. Comparison of Experimental Growth Constants(4) and the Predictions of the Model

zone	growth constant, $\mu m/s^{\frac{1}{2}}$ experimental	theoretical
2	16.2	16.4 ± 1.8
4	5.4	4.6 ± 1.1
5	2.0	3.1 ± 0.5

REFERENCES

1. M. W. Mallett et al., BMI-1210 (1957)

2. D. M. Rooney and L. M. Grossman, GEAP-4679 (1965)

3. S. L. Seiffert, U. S. N. R. C. Report TREE-NUREG-1069 (1977)

4. P. Hofmann and C. Politis, J. Nucl. Mater. 87, (1979) 375.

5. P. E. Blackburn, J. Nucl. Mater., 46, (1973) 244.

6. G. H. Winslow, High Temp. Sci. 7, (1975) 81.

7. O. Kubacheveski, E. Evans and C. B. Alcock, "Metallurgical Thermochemistry", p. 429, Pergammon Press, (1967).

8. R. E. Pawel, J. Electrochem., Soc., 126, (1979) 1111.

9. J. B. Clark and F. N. Rhines, Trans. Amer. Soc. Metals, 51 (1959) 199.

10. A. W. Cronenberg and M. S. El-Genk, J. Nucl. Mater., 78, (1978) 390.

11. G. W. Roper and D. P. Whittle, Metal Sci. 15, (1981) 148.

12. G. H. Winslow, High Temp. Sci. 5 (1973) 1976.

13. R. E. Fryxell et al., J. Nucl. Mater., 25, (1968) 97.

14. J. Crank, "Mathematics of Diffusion", Second Ed. Chap. VIII, Oxford (1975).

15. J. S. Kirkaldy and L. C. Brown, Can. Metallurgical Quart., 2, (1963) 89.

16. G. W. Roper and D. P. Whittle, "Multicomponent Diffusion" LBL-9758 (1979).

17. G. A. Reymann and D. L. Hagrman, "MATPRO - A Handbook of Materials Properties for Use in the Analysis of Light Water Reactor Fuel Rod Behavior", TREE-NUREG-1180 (1978).

18. M. Hansen, "Constitution of Binary Alloys", 2nd Ed., McGraw-Hill (1958).

19. A. V. Grosse, J. A. Cahill and A. D. Kirschenbaum, J. Amer. Chem. Soc. 83 (1961) 4665.

20. S. W. Strauss, Nucl. Sci. & Engin., 18 (1964) 280.

21. D. R. Olander, J. Nucl. Mater., Submitted.

22. Rosa Yang, J. Hovingh, E. LeBorgne and D. R. Olander, High Temp. Sci., 7 (1975) 55.

23. J. Finucane and D. R. Olander, High Temp. Sci. 1 (1969) 2513.

FIGURE CAPTIONS

1. Layers found in the UO_2-Zircaloy interaction after 30 minutes contact at 1400°C (after Ref. 4).
2. The U-Zr-O phase diagram at 1500°C (after Ref. 4)
3. Model of the UO_2-Zircaloy interaction

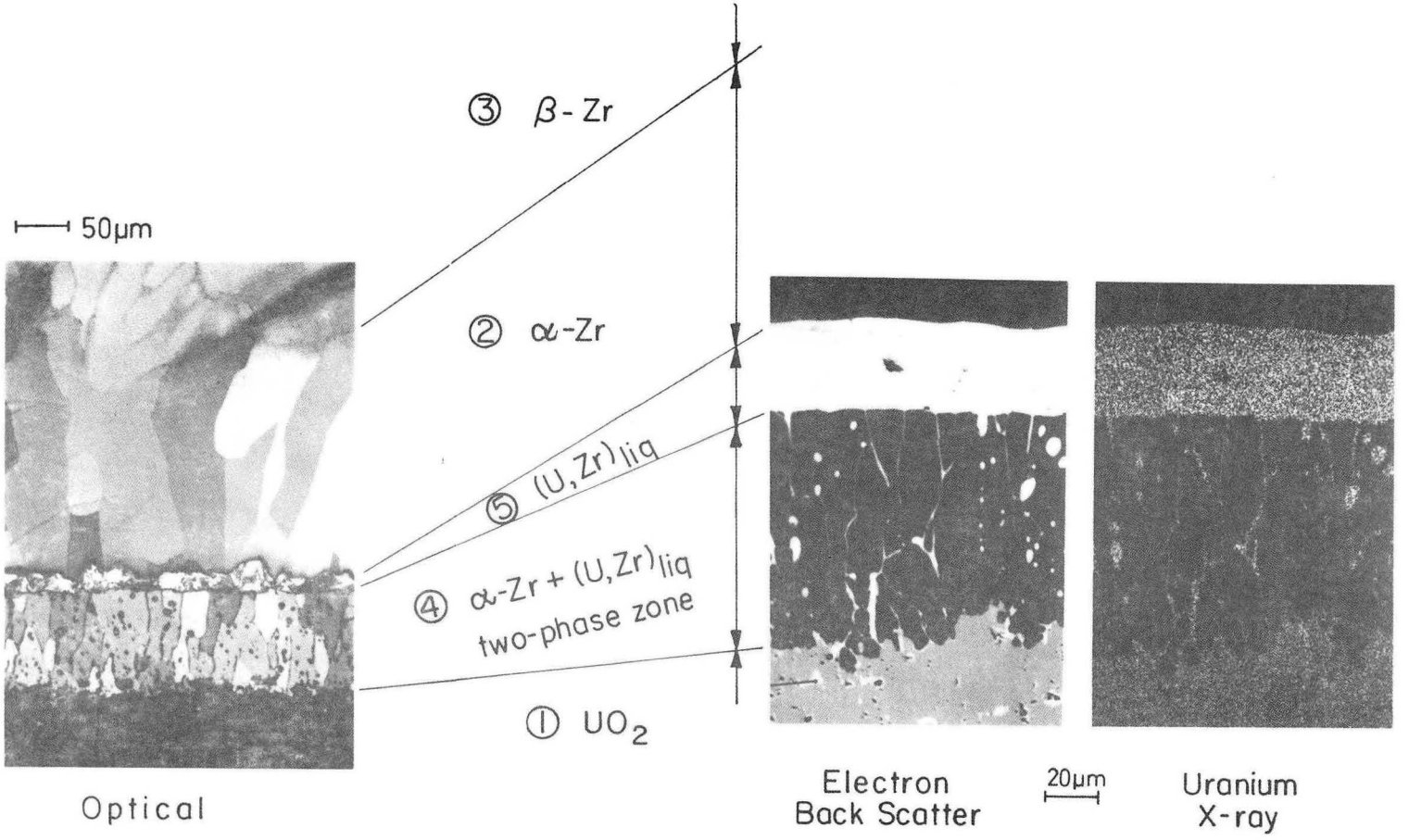

XBB 824-4030

Figure 1.

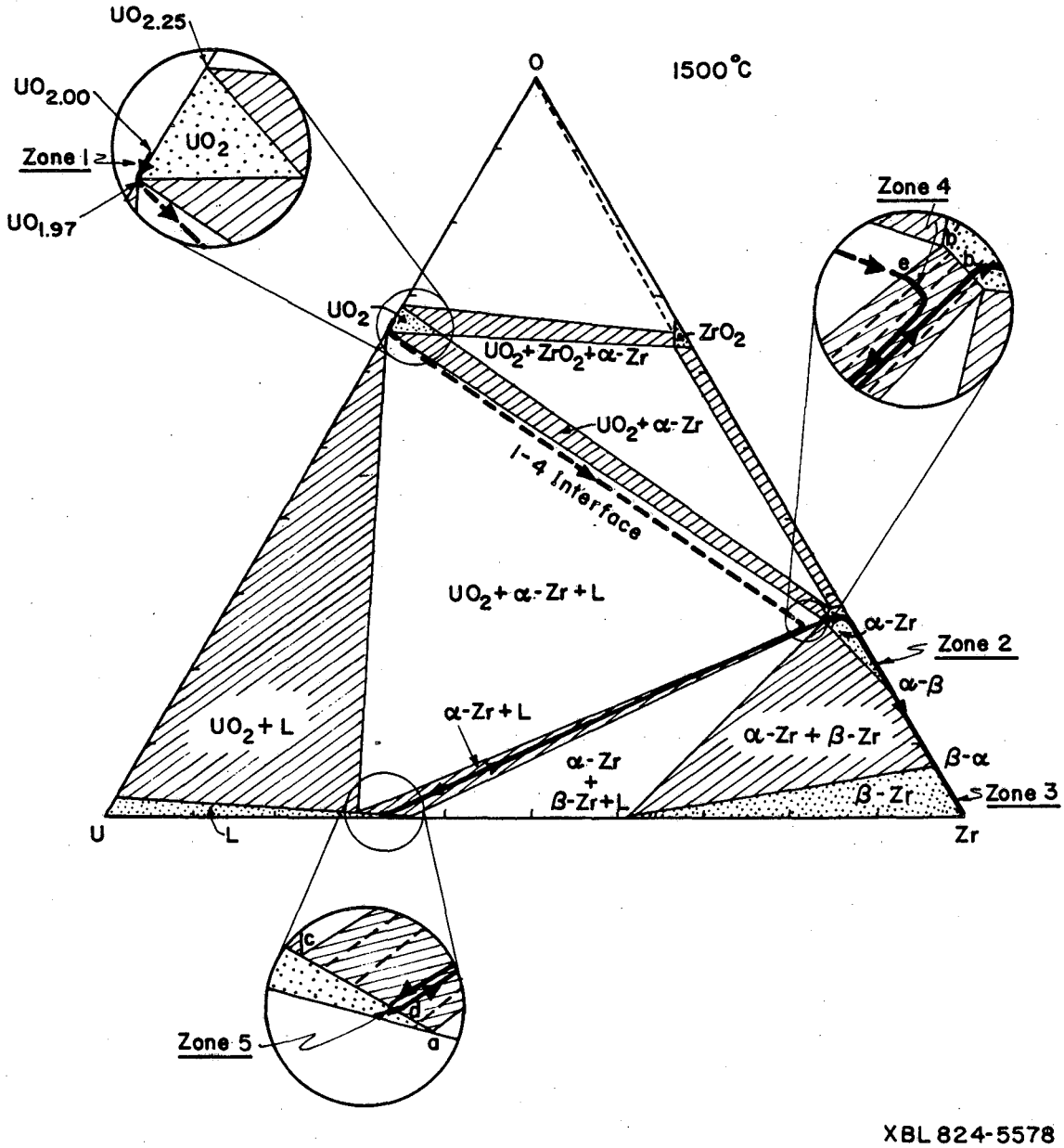
UO2.25
UO2.00
Zone 1
UO1.97
UO2
O
1500°C
Zone 4
e
b
UO2
ZrO2
UO2+ZrO2+α-Zr
UO2+α-Zr
1-4 Interface
UO2+α-Zr+L
α-Zr
Zone 2
α-β
UO2+L
α-Zr+L
α-Zr+β-Zr
β-α
α-Zr
+
β-Zr+L
β-Zr
Zone 3
U
L
Zr
c
d
a
Zone 5
XBL 824-5578

Figure 2.

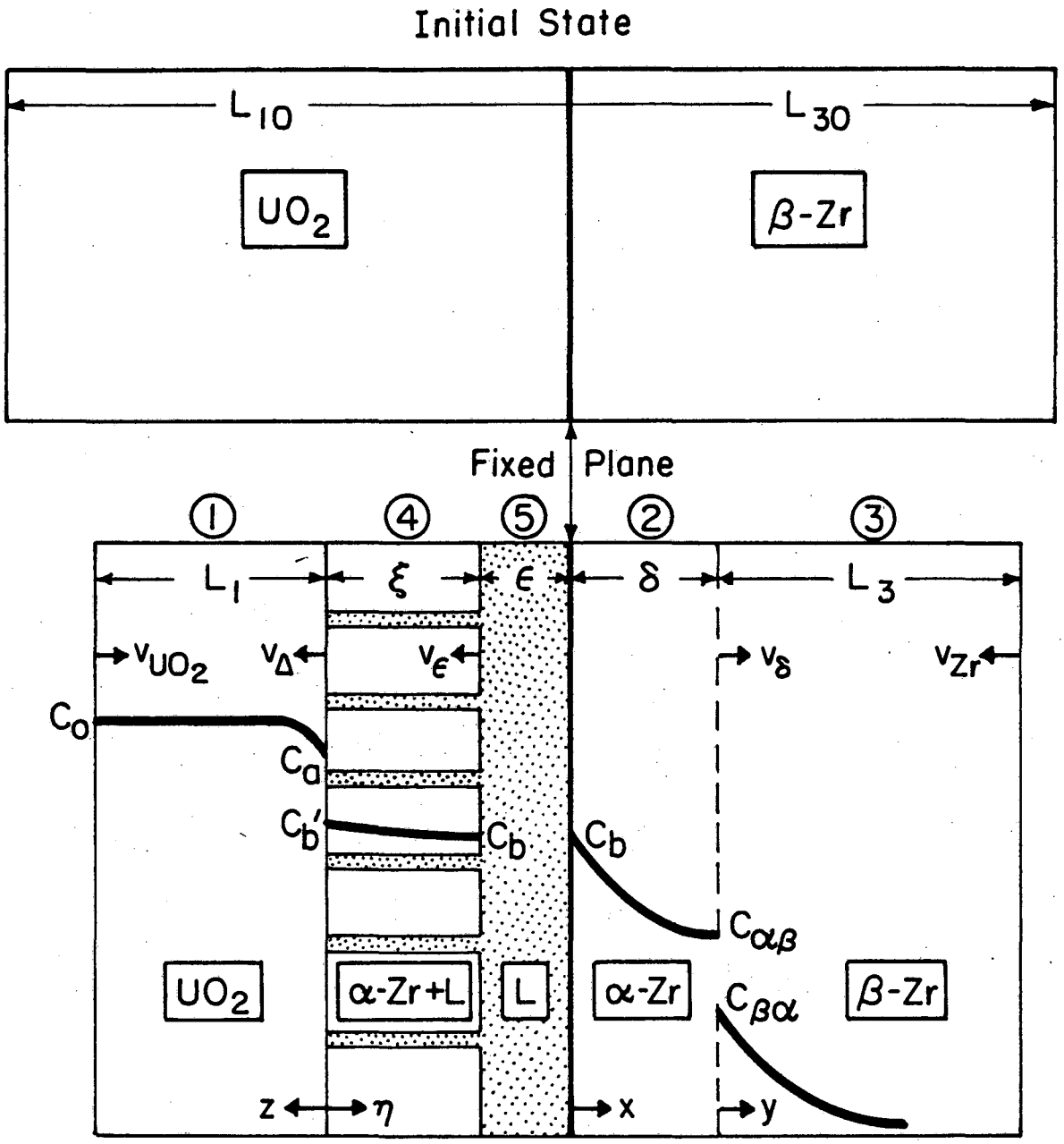
Initial State
L10
L30
UO2
β-Zr
Fixed Plane
1
4
5
2
3
L1
ξ
ε
δ
L3
vUO2
vΔ
vε
vδ
vZr
Co
Ca
Cb'
Cb
Cb
Cαβ
Cβα
UO2
α-Zr+L
L
α-Zr
β-Zr
z
η
x
y
XBL 824-5577

Figure 3.

This report was done with support from the Department of Energy. Any conclusions or opinions expressed in this report represent solely those of the author(s) and not necessarily those of The Regents of the University of California, the Lawrence Berkeley Laboratory or the Department of Energy.

Reference to a company or product name does not imply approval or recommendation of the product by the University of California or the U.S. Department of Energy to the exclusion of others that may be suitable.

TECHNICAL INFORMATION DEPARTMENT
LAWRENCE BERKELEY LABORATORY
UNIVERSITY OF CALIFORNIA
BERKELEY, CALIFORNIA 94720